Annealing-dependent structural and magnetic properties of nickel oxide (NiO) nanoparticles in a silica matrix

Nikolic, Dobrica; Panjan, Matjaz; Blake, Graeme R.; Tadic, Marin

Published in:
Journal of the European Ceramic Society

DOI:
10.1016/j.jeurceramsoc.2015.06.024

Journal of the European Ceramic Society 35 (2015) 3843–3852

Contents lists available at www.sciencedirect.com

Journal of the European Ceramic Society

journal homepage: www.elsevier.com/locate/jeurceramsoc

Annealing-dependent structural and magnetic properties of nickel oxide (NiO) nanoparticles in a silica matrix

Dobrica Nikolić[a], Matjaž Panjan[b], Graeme R. Blake[c], Marin Tadić[d,*]

[a] Department of Physics, Faculty of Mining and Geology, University of Belgrade, Belgrade, Serbia
[b] Jozef Stefan Institute, Jamova 39, 1000 Ljubljana, Slovenia
[c] Zernike Institute for Advanced Materials, University of Groningen, Nijenborgh 4, 9747 AG Groningen, The Netherlands
[d] Condensed Matter Physics Laboratory, Vinča Institute of Nuclear Sciences, University of Belgrade, POB 522, Belgrade 11001, Serbia

ARTICLE INFO

Article history:
Received 4 March 2015
Received in revised form 13 June 2015
Accepted 21 June 2015
Available online 9 July 2015

Keywords:
Nickel oxide (NiO)
Sol–gel combustion synthesis
Interparticle interactions
Superparamagnetism
AC susceptibility

ABSTRACT

We show that annealing at high temperatures has a significant effect on the structural and magnetic properties of NiO/SiO_2 nanostructures synthesized by a sol–gel combustion method. Samples underwent heat treatments at 500 °C, 800 °C, 950 °C and 1100 °C. As compared to the 500 °C sample, the 800 °C sample showed the following magnetic properties: much higher irreversibility temperature, a significantly broadened zero-field-cooled (ZFC) magnetization maximum, a decrease of the ZFC magnetization, an increase of the coercivity, and weaker inter-particle interactions. These changes can be attributed to agglomeration of nanoparticles in part of the sample. We believe that this agglomeration can be explained by the removal of thin regions of silica that separate nanoparticles in close proximity during the annealing process at 800 °C. Magnetic measurements for the 1100 sample reveal both an abrupt increase in size of the NiO nanoparticles, which is confirmed by TEM and XRPD measurements, and an increase in inter-particle interaction strength.

1. Introduction

Interest in the magnetic properties of nanosized NiO has recently been revived due to reports of interesting and complex magnetic behavior [1–16]. Although bulk NiO is antiferromagnetic, nanoparticles exhibit room-temperature coercivity, spin-glass behavior, superparamagnetism, memory effects, exchange bias effects and magnetic transitions at low temperature [17–29]. The novel magnetic properties of NiO nanoparticles compared to bulk material are mainly due to a complex interplay between finite size effects, surface effects and inter-particle interactions [4,6,16,22,24,27,28]. Finite size effects are related to the reduced number of exchange-coupled spins within nanoparticles, whereas surface effects are related to the reduced symmetry of surface atoms. Moreover, for agglomerated magnetic nanoparticles, magnetostatic interactions have a high impact on the magnetic behavior and slow down the relaxation time τ of the magnetic moments [22,30]. It has been reported that inter-particle interactions between magnetic nanoparticles in close proximity strongly affect the macroscopic magnetic properties, giving rise to phenomena such as an increase of the blocking temperature T_B, broadening of the magnetization maximum, changed values of coercivity and magnetization, and spin glass behavior. Therefore, the magnetic properties of agglomerated magnetic nanoparticles are strongly influenced by inter-particle interactions and differ significantly from those of isolated nanocrystals. Accordingly, one particularly interesting topic is the study of inter-particle interactions of NiO nanoparticles. Winkler et al. investigated the effect of interactions between ~3 nm NiO nanoparticles by comparing the magnetic properties of a powder sample (interacting particles) with a sample in which the particles were dispersed in a polymer (weakly interacting sample) [22]. They revealed that inter-particle interactions shift the distribution of blocking temperatures to higher temperatures and increase the effective energy barriers of the particles. They also found that the magnetization of the powder sample was much lower, implying that inter-particle interactions have a demagnetizing effect [22]. Bodker et al. showed that inter-particle interactions can have a strong effect on the superparamagnetic relaxation behavior of NiO nanoparticles [31]. They found that the ZFC maximum is broadened as the interaction strength increases and that the upturn in the FC curve at low temperatures is suppressed [31]. Meneses et al. also studied the magnetic properties of NiO nanoparticles with different strengths of inter-particle inter-

* Corresponding author at: Condensed Matter Physics Laboratory, Vinca Institute, P.O. Box 522, 11001 Belgrade, Serbia. Fax: +381 11 6308829.
E-mail address: marint@vinca.rs (M. Tadić).

http://dx.doi.org/10.1016/j.jeurceramsoc.2015.06.024
0955-2219/

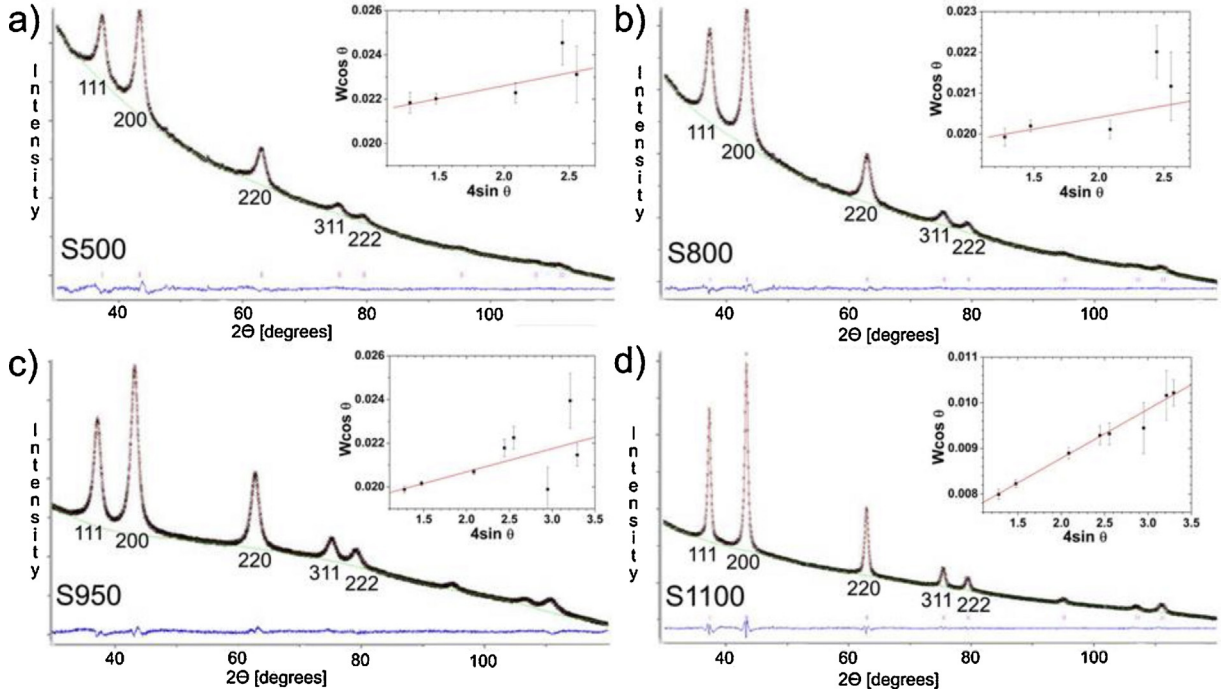

Fig. 1. Observed (points), calculated (line) and difference (bottom line) X-ray powder diffraction patterns of samples S500 (a), S800 (b), S950 (c) and S1100 (d). The insets show Williamson–Hall plots based on the five labelled peaks, with a linear fit (red lines).(For interpretation of the reference to color in this figure legend, the reader is referred to the web version of this article.)

actions [32]. They revealed two maxima in the ZFC magnetization curves, the lower of which was not magnetic field dependent but depended strongly on the inter-particle interaction strength [32].

Recently, the properties of magnetic nanoparticles in various matrixes have been widely studied due to fundamental and technological interest [33–35]. These systems are useful for investigation of the relationship between the size of the particles, inter-particle interactions and macroscopic magnetic properties [36–42]. However, thus far no detailed studies have been carried out to investigate the effect of annealing at high temperatures on the magnetic properties of NiO nanoparticles in a silica matrix. In this work, we present an investigation of the structural and magnetic properties of NiO/SiO_2 nanostructures after annealing treatment at high temperatures (500 °C, 800 °C, 950 °C and 1100 °C). Our results suggest that agglomeration of the NiO nanoparticles during the annealing process at 800 °C has an important effect on the magnetic behavior. The observed magnetic properties of the NiO nanoparticles are complex and are strongly affected by the temperature-dependent interplay between finite size effects and inter-particle interactions.

2. Experimental

The NiO nanoparticles in a silica matrix were prepared using a sol–gel combustion method [14]. In brief, the starting point for the synthesis of this targeted system was a solution prepared by mixing tetraethoxysilane (TEOS, Aldrich), distilled water, ethanol, nickel nitrate ($Ni(NO_3)_2{\cdot}6H_2O$, Aldrich) and citric acid monohydrate (CA, Aldrich). Nickel nitrate was added to the initial solution in such a proportion as to provide 25 wt.% of nickel oxide in the final dried powder. The molar ratios of ethanol to TEOS, water to TEOS and nickel nitrate to CA were 4:1, 12:1, and 1:0.9, respectively. The pH of the mixture was adjusted to about 2.5 after an hour of stirring. The sol was dried for about 35 h at 55 °C. The gel was subsequently heated in air at 500 °C (S500), 800 °C (S800), 950 °C (S950) and 1100 °C (S1100) for three hours.

The crystalline part of the samples was analyzed using X-ray powder diffraction (XRPD) on a Bruker D8 Advance diffractometer operating with Cu Kα radiation. Measurements were performed in the range $10° \leq 2\theta \leq 120°$. The chemical composition was determined using energy-dispersive X-ray spectroscopy (EDS) implemented in a field emission scanning electron microscope (FE-SEM, JEOL JSM-7600F). The size and distribution of the nickel oxide nanoparticles were observed using a high resolution transmission electron microscope (JEOL 2010-F) operating at 200 kV. Magnetic measurements were performed on a commercial Quantum Design MPMS-XL-5 SQUID-based magnetometer over a wide range of temperatures (5–300 K) and applied DC fields (up to 5 T). The same instrument was used for AC magnetization measurements carried out in the $1\,Hz \leq \nu \leq 1000\,Hz$ frequency range in the temperature range encompassing the maxima in the magnetization curves.

3. Results and discussion

The labels S500, S800, S950, S1100, used below in the text, indicate the final heat treatment temperatures. All the samples were characterized by XRPD measurements (Fig. 1), which confirm the formation of the NiO crystal structure with space group *Fm*-3*m* [28,43,44]. The XRPD patterns were fitted in the range $30° \leq 2\theta \leq 120°$ using the GSAS software [45]. The refined lattice parameter of NiO was 4.1714(10) Å, 4.1790(5) Å, 4.1840(3) Å, and 4.1818(2) Å for the S500, S800, S950 and S1100 samples, respectively. The strong upturn in the background towards lower diffraction angles can be attributed to the amorphous silica matrix. The full widths at half maximum W of the five to eight lowest angle peaks, corrected for the instrumental peak width (determined using a standard LaB_6 sample), were used to construct Williamson–Hall plots of $W\cos\theta$ versus $4\sin\theta$ as shown in the insets to Fig. 1. Estimates of the volume-weighted average crys-

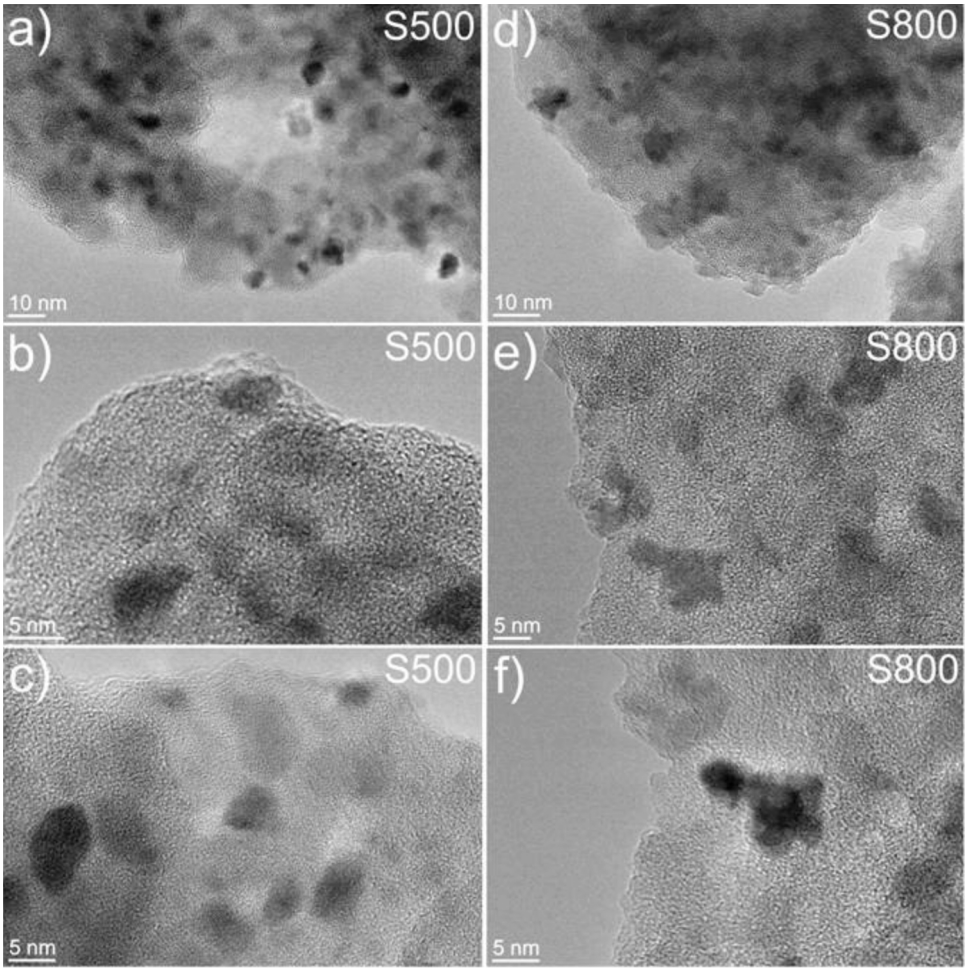

Fig. 2. Transmission electron micrographs of S500 and S800.

tallite sizes D can then be obtained from linear fits to the data; the intercept is $K\lambda/D$, where K is the shape factor (∼0.9) and λ is the X-ray wavelength (1.5406 Å). The average crystallite sizes obtained from the fits were $D = 7.0(5)$ nm for S500, $D = 7.6(4)$ nm for S800 $D = 7.5(2)$ nm for S950, and $D = 21(2)$ nm for S1100. The EDS measurements of the samples confirmed that Ni, Si and O are the main components with atomic ratios in good agreement with those expected from the synthesis conditions. The size, morphology and microstructure of the nanoparticles were investigated by TEM and HRTEM measurements, as shown in Figs. 2 and 3. It can be seen that the nanoparticles in all samples are embedded in a silica matrix. The TEM images reveal that the diameters of both the S500 and S800 nanoparticles are about 7 nm (Fig. 2), consistent with the XRPD analysis. Moreover, annealing at 800 °C gives rise to agglomeration of the nanoparticles (Fig. 2(d–f)). We believe that thin regions of the silica matrix that separate nanoparticles in close proximity are removed during annealing at 800 °C, allowing direct contact between nanoparticles. Therefore, both well-isolated and agglomerated nanoparticles are identified in the S800 sample (Fig. 2(d–f)). Our TEM measurements show minimal or no aggregation between NiO nanoparticles in the S500 sample (Fig. 2(a–c)). Compagnini et al. studied a system comprised of silver nanoparticles embedded in silica and also observed degradation of the silica matrix after thermal treatments at temperatures above 500 °C, with the formation of voids and extended defects in the matrix and an increase in size of the nanoparticles [46]. Our work shows that the NiO/SiO_2 nanostructure exhibits similar behavior, suggesting that this effect might be common for nanosized materials embedded in a silica matrix. In Fig. 3(a–c), we can see isolated and agglomerated nanoparticles as well as the formation of bigger grains in the S950 sample. The TEM images of sample S1100 (Fig. 3(d–f)) show an abrupt increase in the size of NiO nanoparticles, as also observed by XRPD. Particle size histograms determined from several TEM images are presented in Fig. 4. The histograms were fitted using a log-normal distribution of particle diameters from which the mean particle diameter <D> and the distribution width δ were determined (Fig. 4). We obtained $\langle D\rangle_{S500} = 6.4$ nm and $\delta_{S500} = 0.19$ for S500, $\langle D\rangle_{S800} = 6.6$ nm and $\delta_{S800} = 0.35$ for S800, $\langle D\rangle_{S950} = 6.7$ nm and $\delta_{S950} = 0.36$ for S950, and $\langle D\rangle_{S1100} = 12.7$ nm and $\delta_{S1100} = 0.42$ for S1100. We thus observe an increase of the mean particle diameter and distribution width with increasing annealing temperature. The values of <D> and δ are very similar for the samples S800 and S950, whereas δ is much smaller for sample S500 and considerably higher for sample S1100. The histogram of sample S1100 indicates significantly larger particles compared to the other samples.

In order to investigate the dynamic behavior of the magnetization in the samples, AC susceptibility measurements were performed at four different frequencies of 1, 25, 100 and 1000 Hz, over the temperature range that encompasses the AC susceptibility maxima. From the experimental data presented in Figs. 5 and 6, it can be seen that the in-phase component $\chi'(T)$ of all four samples exhibits a peak that increases in temperature with increasing frequency, while the height of the peak decreases. These data provide insight into the nature of inter-particle interactions in the sam-

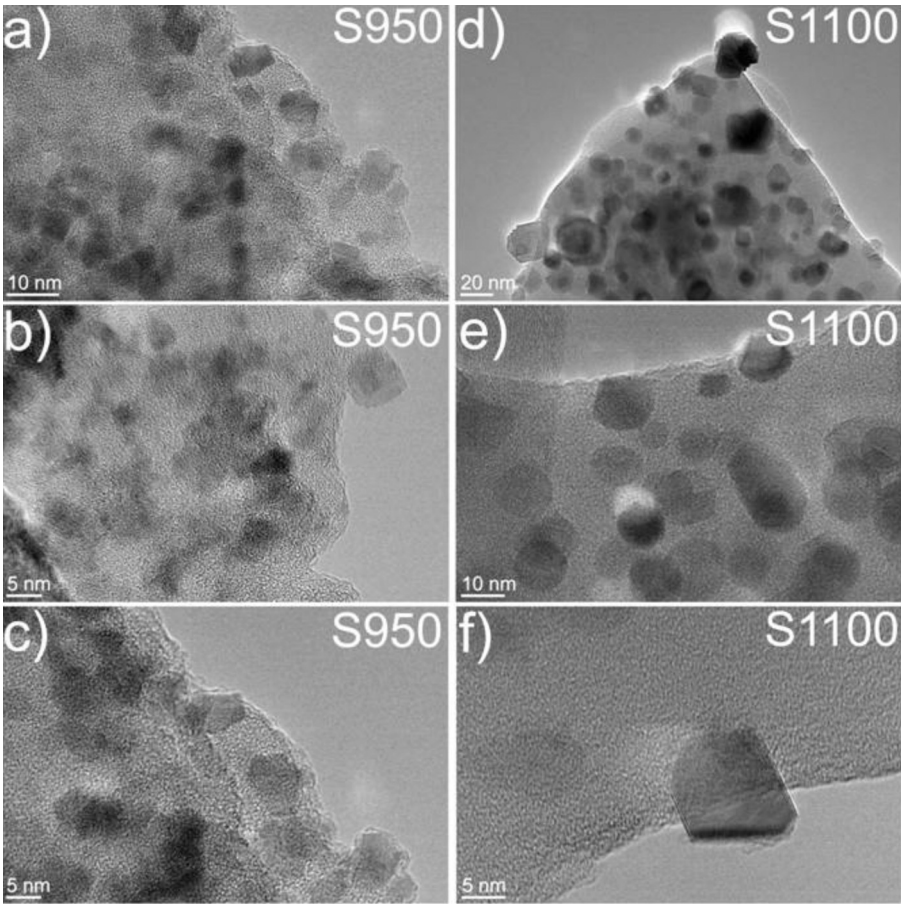

Fig. 3. Transmission electron micrographs of S950 and S1100.

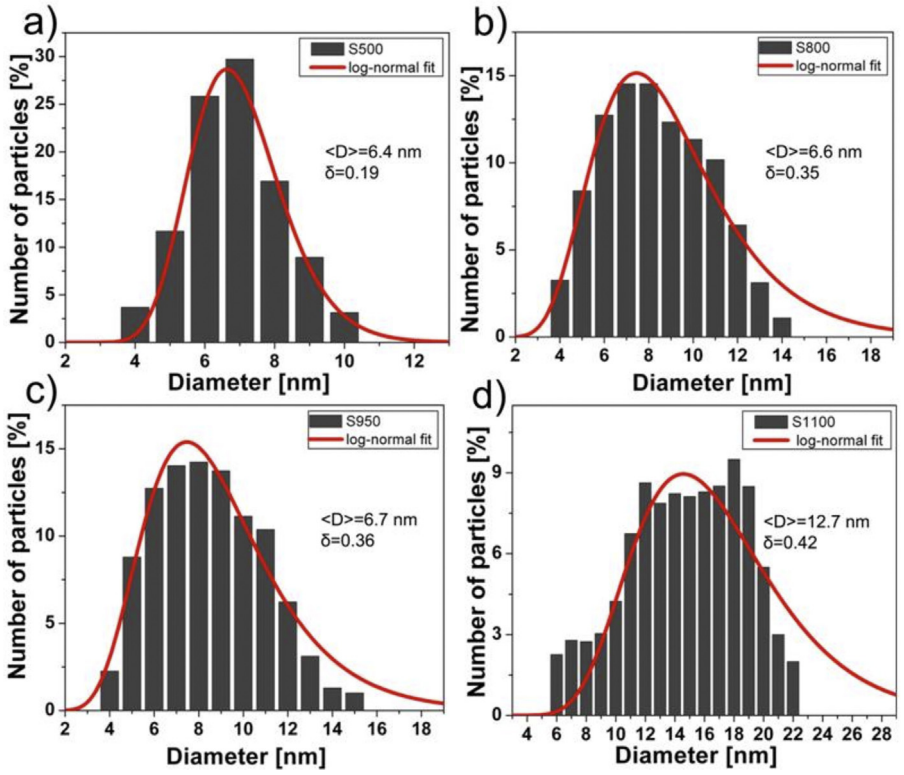

Fig. 4. Particle size histograms of the samples fitted by log-normal distribution function.

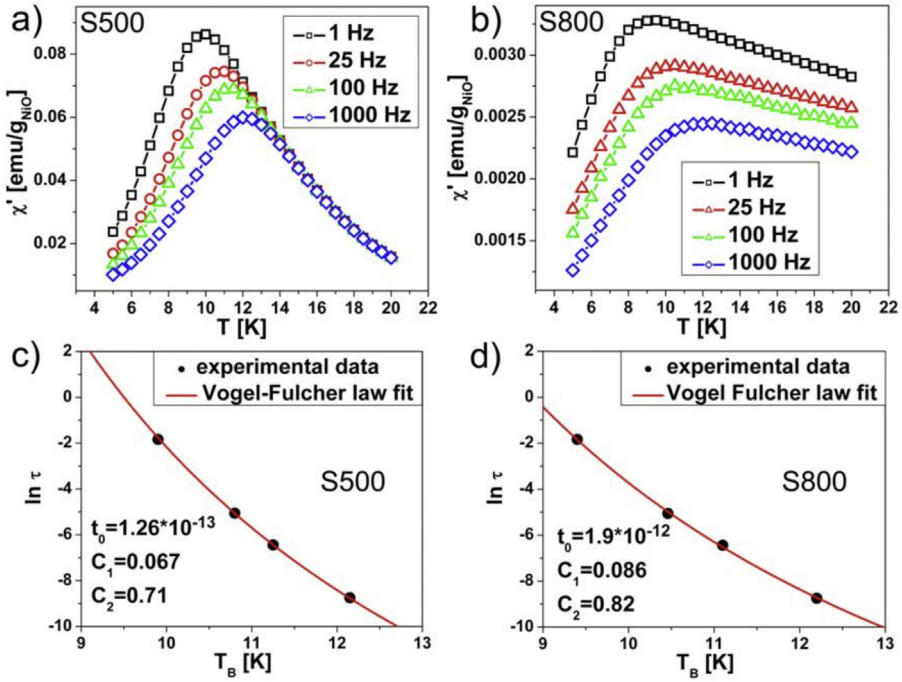

Fig. 5. In-phase component of the AC susceptibility χ' as a function of temperature for various frequencies with corresponding fits to the Vogel–Fulcher law for the samples S500 (a and c) and S800 (b and d).

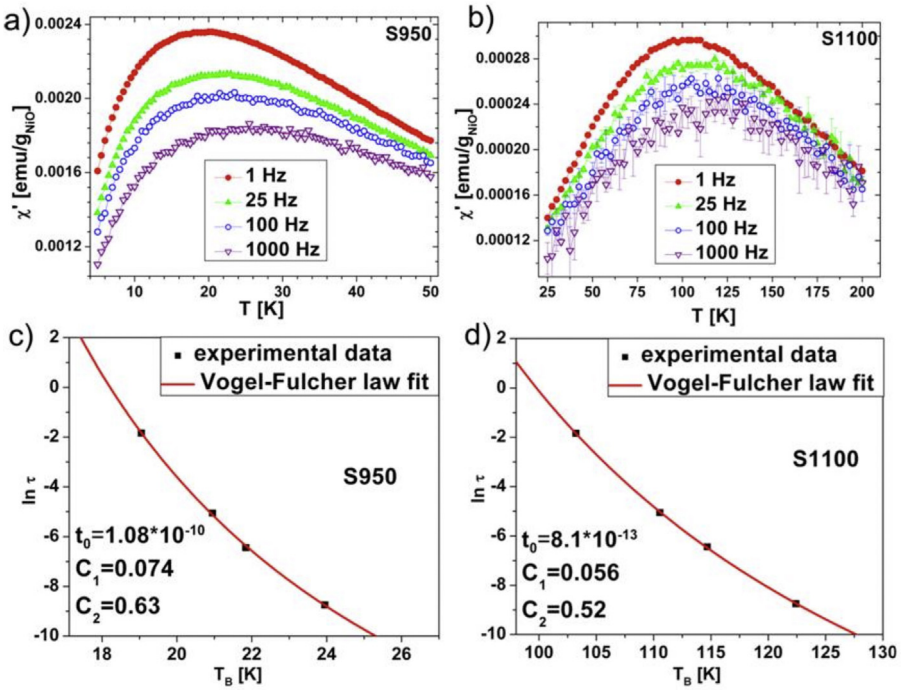

Fig. 6. In-phase component of the AC susceptibility χ' as a function of temperature for various frequencies with corresponding fits to the Vogel–Fulcher law for the samples S950 (a and c) and S1100 (b and d).

ples. A useful criterion for distinguishing between freezing and blocking processes lies in determining the relative shift in temperature per decade frequency by extracting the empirical parameter $C_1 = \Delta T_B/(T_B \Delta \log \nu)$ [34]. The values obtained were $C_{1(S500)} = 0.067$, $C_{1(S800)} = 0.086$, $C_{1(S950)} = 0.074$ and $C_{1(S1100)} = 0.056$. The expected value of C_1 for non-interacting particles lies in the range ~0.1–0.13, whereas for spin glasses $C_1 < 0.03$ [47,48]. Therefore, our data indicate the existence of inter-particle interactions in all samples and the maxima in $\chi'(T)$ correspond to the blocking temperatures T_B.

The frequency dependence of the $\chi'(T)$ maxima (Fig. 5 and 6(a,b)) can then be fitted to the Vogel–Fulcher law (Figs. 5 and 6(c–d)) [24,30,32]:

$$\Gamma = \Gamma_0 \exp\left[\frac{E_a}{k_B}(T_B - T_0)\right] \quad (1)$$

where E_a is the energy barrier to magnetization reversal in a single particle, $\tau = 1/\nu$ is the characteristic time of the experiment (ν is the frequency of the magnetic field) and T_0 is a measure

Table 1
Magnetic parameters of the samples.

Sample	τ_0 [s]	E_a [K]	T_0 [K]	K_{eff} [erg/cm^3]	C_1	C_2
S500	1.26×10^{-13}	187.8	3.18	1.89×10^5	0.067	0.71
S800	1.9×10^{-12}	187.1	1.96	1.72×10^5	0.086	0.82
S950	1.08×10^{-10}	225.7	8.2	1.21×10^5	0.074	0.63
S1100	8.1×10^{-13}	1298	53.78	1.7×10^5	0.056	0.52

of the inter-particle interaction strength. The best fits of the experimental data to Eq. (1) are shown in Figs. 5 and 6(c–d), from which the following parameters were extracted: $\tau_{0(S500)} = 1.26 \times 10^{-13}$ s, $E_{a(S500)}/k_B = 187.8$ K, $T_{0(S500)} = 3.18$ K for S500; $\tau_{0(S800)} = 1.9 \times 10^{-12}$ s, $E_{a(S800)}/k_B = 187.1$ K, $T_{0(S800)} = 1.96$ K for S800; $\tau_{0(S950)} = 1.08 \times 10^{-10}$ s, $E_{a(S950)}/k_B$=225.7 K, $T_{0(S950)}$ = 8.2 K for S950; $\tau_{0(S1100)} = 8.1 \times 0^{-13}$ s, $E_{a(S1100)}/k_B = 1298$ K, $T_{0(S1100)} = 53.78$ K for S1100. The magnetic anisotropy parameter of a nanoparticle E_a/k_B can be used to estimate the effective anisotropy constant K_{eff} using the relation $K_{eff}V = E_a$, where V is the volume of the particle. For spherical particles with diameters of $d_{(S500)}$ =6.4 nm and $d_{(S800)} = 6.6$ nm, this relation gives $K_{eff(S500)} = 1.89 \times 10^5$ erg/cm^3, $K_{eff(S800)} = 1.72 \times 10^5$ erg/cm^3, $K_{eff(S950)} = 1.21 \times 10^5$ erg/cm^3 and $K_{eff(S1100)} = 1.7 \times 10^5$ erg/cm^3. These values of K_{eff} are in good agreement with previous reports for nanocrystalline NiO [28,49]. In order to further analyze the AC susceptibility data, we calculated the value of another empirical parameter $C_2 = (T_B - T_0)/T_B$ using the T_0 values obtained from the Vogel–Fulcher fit. The obtained values were $C_{2(S500)} = 0.71$, $C_{2(S800)} = 0.82$, $C_{2(S950)} = 0.63$ and $C_{2(S1100)} = 0.52$, whereas the expected value of the C_2 parameter for non-interacting systems is about one [47,48]. These values are in agreement with literature data for interacting nanoparticle systems [50–52]. The determined magnetic parameters of the samples are summarized in Table 1.

The annealing treatment has a significant effect on the nature of the inter-particle interactions. As compared to the S500 sample, the sample annealed at 800 °C showed significantly weaker inter-particle interactions based on the frequency dependence of the maximum in the AC susceptibility. It should also be noted that the χ'(T) maximum in the S800 sample is much broader than in the S500 sample (Fig. 5(a) (S500) and (b) (S800)). This indicates that there is a broad distribution of anisotropy energy barriers for the S800 nanoparticles. Our observations can be explained by the annealing-induced agglomeration of nanoparticles that are in close proximity to each other (Fig. 2(a–c)), resulting in the S800 sample containing populations of both well-isolated and agglomerated nanoparticles (Fig. 2(d–f)). We may conclude that the maximum in χ' (T) for the S800 sample (Fig. 5(b), $T_{max} = 8$ K) corresponds to the blocking temperature of the fraction of nanoparticles that are well-isolated; this peak is strongly broadened by the fraction of nanoparticles that are agglomerated. The determined values of C_1 and C_2 for S950 are close to those of S500. However, the values of C_1 and C_2 for S1100 are smaller than those of the other samples investigated in this work, indicating stronger inter-particle interactions, which is in agreement with the field-cooled magnetization data discussed below.

We also measured the field-cooled (FC) and zero-field-cooled (ZFC) DC magnetic susceptibility of all samples as a function of temperature between 5 K and 100 K (Fig. 7). The measurements were performed in an applied magnetic field of $H = 100$ Oe on warming after the sample had been cooled either in the absence (ZFC curve) or presence (FC curve) of the same applied magnetic field. At high temperatures, the ZFC and FC curves overlap and the susceptibility increases with decreasing temperature. However, the two curves separate below an irreversibility temperature. In order to assign values of T_{irr}, we first chose different dM values and determined the temperatures at which the ZFC and FC curves are separated by these values, as shown in Table 2. It is apparent that T_{irr} depends on the choice of dM; an increase of dM gives a decrease of T_{irr}. The

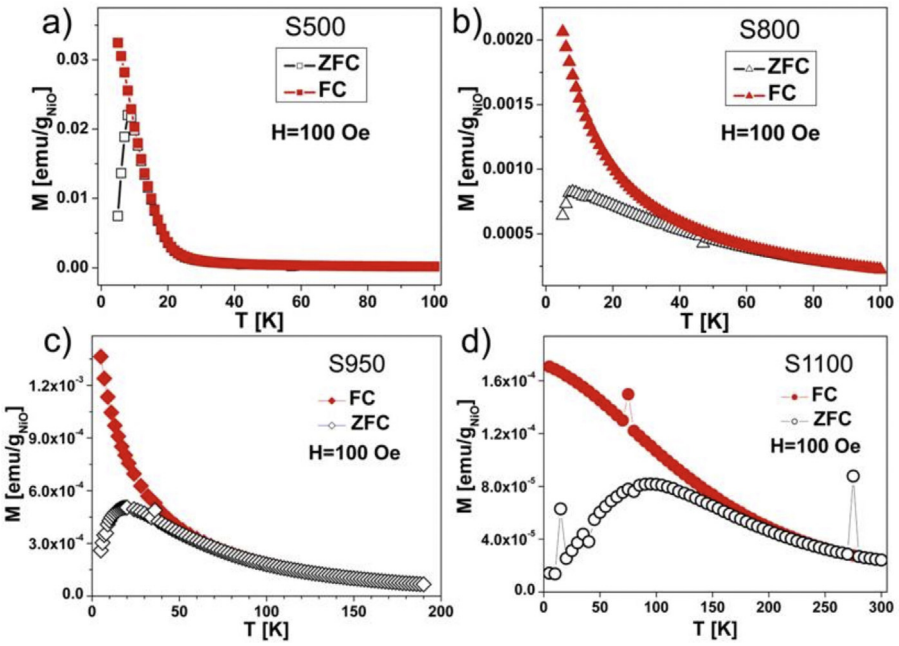

Fig. 7. Field-cooled and zero-field-cooled magnetization as a function of temperature for (a) S500, (b) S800, (c) S950 and (d) S1100 under an applied magnetic field of 100 Oe.

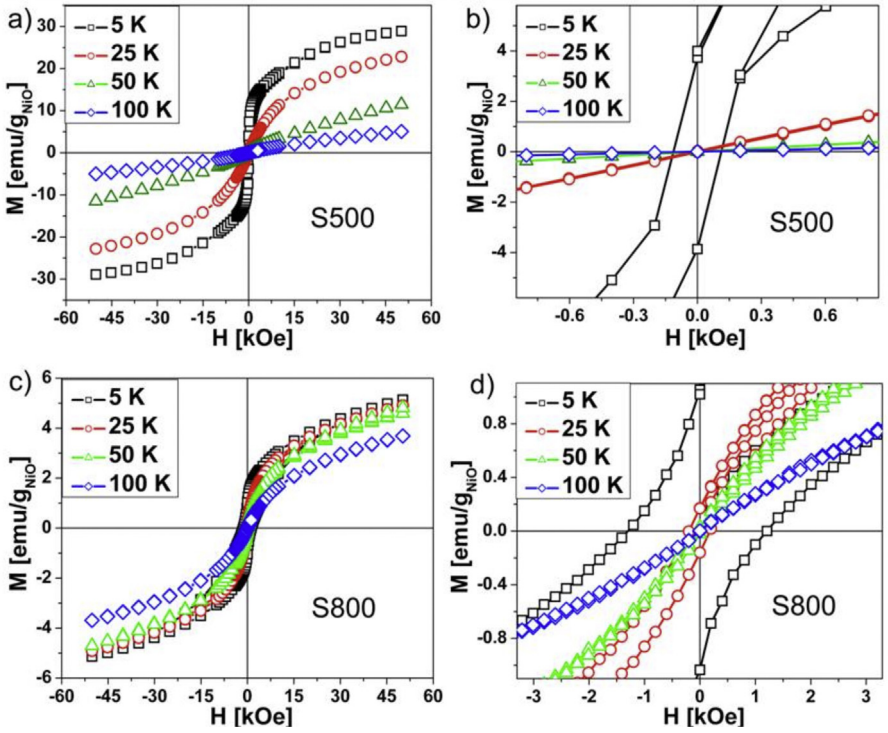

Fig. 8. Dependence of the isothermal magnetization M(H) of the samples S500 (a and b) and S800 (c and d) at the indicated temperatures.

Table 2
Dependence of irreversibility temperature on different chosen magnetization values dM.

	dM [emu/g]	dM [emu/g]	dM [emu/g]	dM [emu/g]
	0.05×10^{-5}	0.1×10^{-5}	0.2×10^{-5}	0.5×10^{-5}
$T_{irr(S500)}$ [K]	51	47	39	31
$T_{irr(S800)}$ [K]	87	78	65	56
$T_{irr(S950)}$ [K]	90	74	67	54
$T_{irr(1100)}$ [K]	255	200	155	115

most sensitive dependence of T_{irr} on dM was observed for the S1100 sample.

We define T_{irr} as the point where the ratio $(M_{FC}–M_{ZFC})/M_{FC}$ becomes less than 1%. Using this criterion, we determined a T_{irr} of 14 K for S500, 72 K for S800, 82 K for S950 and 255 K for S1100.

The FC susceptibility of all samples increases monotonically with decreasing temperature below T_{irr} whereas the ZFC susceptibility exhibits a maximum at ~8 K for S500 and S800, ~20 K for S950 and ~95 K for S1100, and then sharply decreases at low temperatures. The temperature at which such a maximum in the ZFC curve occurs is usually referred to as the blocking temperature, below which the magnetic moments are frozen in fixed directions or "blocked" [53,54]. The blocking of a superparamagnetic particle is related to its magnetic anisotropy energy E_a [55]. Moreover, the blocking temperature is defined as the temperature at which the relaxation time τ of the magnetic moments is equal to the time-scale of the measurement technique (τ_m) [56]. The relaxation time τ needed to reverse the magnetic moment of a non-interacting particle follows the Arrhenius law $\tau = \tau_0 \exp(E_a/k_B T)$, where $E_a = K_{eff} V$ (K_{eff} is the effective anisotropy constant and V is the particle volume) and τ_0 denotes the attempt frequency [56,57]. Therefore, particles with larger V and K_{eff} will have higher energy barriers E_a. The relaxation times of such particles will thus be longer and their magnetic moments will become blocked at higher temperatures. The broader maxima ($T_{max} \sim 8$ K) in the AC and ZFC measurements for S800 compared to S500 (Figs. 5 and 7(a,b)) imply the existence of a broader energy barrier distribution for these nanoparticles. Moreover, the ZFC and FC curves for S800 remain separated until much higher temperature ($T_{irr} = 72$ K) than S500, which represents the blocking temperature of the particles with the largest energy barrier. The increase of T_{irr} and broadening of the magnetization maximum in S800 compared to S500 could be associated with the part of the sample that consists of agglomerated nanoparticles (bigger grains), as previously reported in the literature [31]. The presence of two particle populations with different inter-particle interactions (well-isolated and agglomerated nanoparticles) would then be associated with complex magnetic relaxation mechanisms, leading to a wide distribution of blocking temperatures.

The determined T_{irr} values are very similar for S800 and S950, which is in agreement with the TEM analysis (Fig. 4). The abrupt increase of the ZFC maximum and T_{irr} in the sample S1100 suggests a significantly larger size of NiO particles, which is confirmed by our TEM (Fig. 3) and XRPD measurements (Fig. 1). Moreover, the ZFC peak is significantly wider in S1100 than in the other samples investigated (Fig. 7(d)), which indicates a wider size distribution. The increase in FC magnetization is somewhat suppressed at low temperature, which is an indication of much stronger inter-particle interactions. In non-interacting and weakly-interacting systems the magnetization rapidly increases with decreasing temperature during FC measurements due to spins which are able to align with the applied field. Inter-particle interactions suppress this alignment and the FC magnetization increases more slowly or becomes flattened at low temperatures.

The field dependence of the magnetization M(H) was measured at four different temperatures for all samples and is shown in Figs. 8 and 9. The magnetization is not saturated in high magnetic fields for any of the samples, as was also observed for other nickel oxide nanomaterials [22]. The hysteresis loops are symmetric around the origin, with coercivity, remanence and saturation magnetization at 5 K of $H_{C(S500)} = 110$ Oe, $M_{r(S500)} = 3.80$ emu/g, and $M_{S(S500)} = 32.85$ emu/g for sample S500 and $H_{C(S800)} = 1250$ Oe, $M_{r(S800)} = 0.96$ emu/g, and $M_{S(S800)} = 6.95$ emu/g for sample S800.

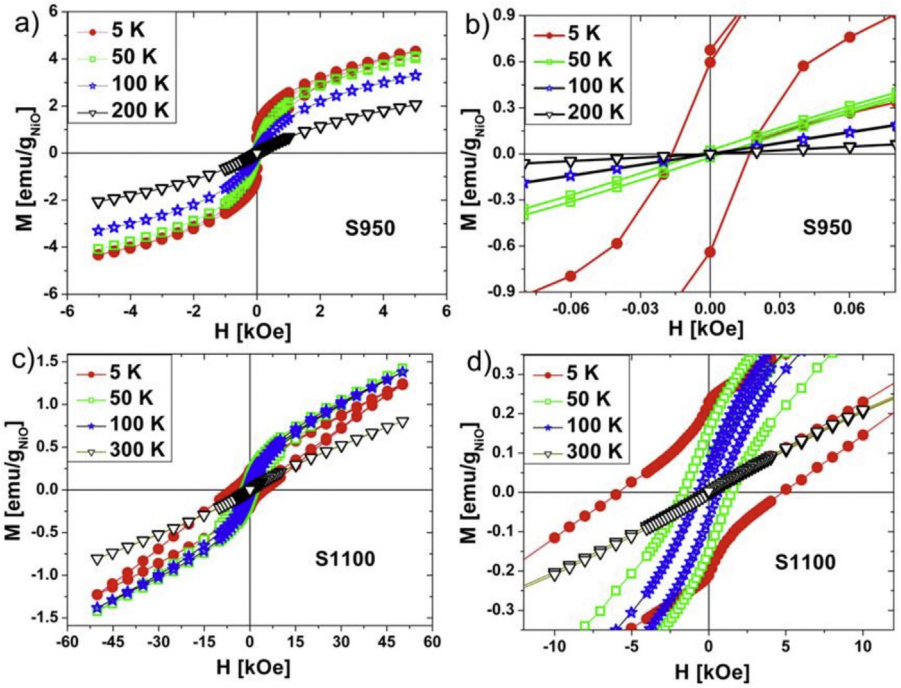

Fig. 9. Dependence of the isothermal magnetization M(H) of the samples S950 (a and b) and S1100 (c and d) at the indicated temperatures.

The values of M_S were determined by extrapolating plots of M versus reciprocal field to 1/H = 0. The S800 sample has a much higher coercive field and a much smaller magnetization than S500 (Fig. 8). An increase of coercive field due to particle agglomeration has previously been reported for NiO nanoparticles [32]. It has also been reported that inter-particle interactions among magnetic nanoparticles increase the energy barrier E_a and enhance H_C [58]. Moreover, much lower magnetization has been reported for interacting NiO nanoparticles in comparison with weakly interacting NiO systems, indicating the demagnetizing character of inter-particle interactions [22]. We thus conclude that agglomeration of the NiO nanoparticles in S800 can produce a decrease in the magnetization and an increase of the coercive field. The M(H) curves recorded at $T = 100$ K for samples S500 and S800 show the absence of both coercivity and remanence, which points to superparamagnetic-like behavior at this temperature (Fig. 8). It should be noted that S500 shows superparamagnetic properties above 25 K (Fig. 8(b)) whereas this is the case only at 100 K for S800 (Fig. 8(d)). The magnetic moments of the nanoparticles m_p in samples S500 and S800 were determined from the equation $m_p = M_S \rho V$, where $\rho = 6.67\ g/cm^3$ is the density of the nanoparticles, and $V_{(S500)} = 164.64 \times 10^{-21}\ cm^3$ and $V_{(S800)} = 195.43 \times 10^{-21}\ cm^3$

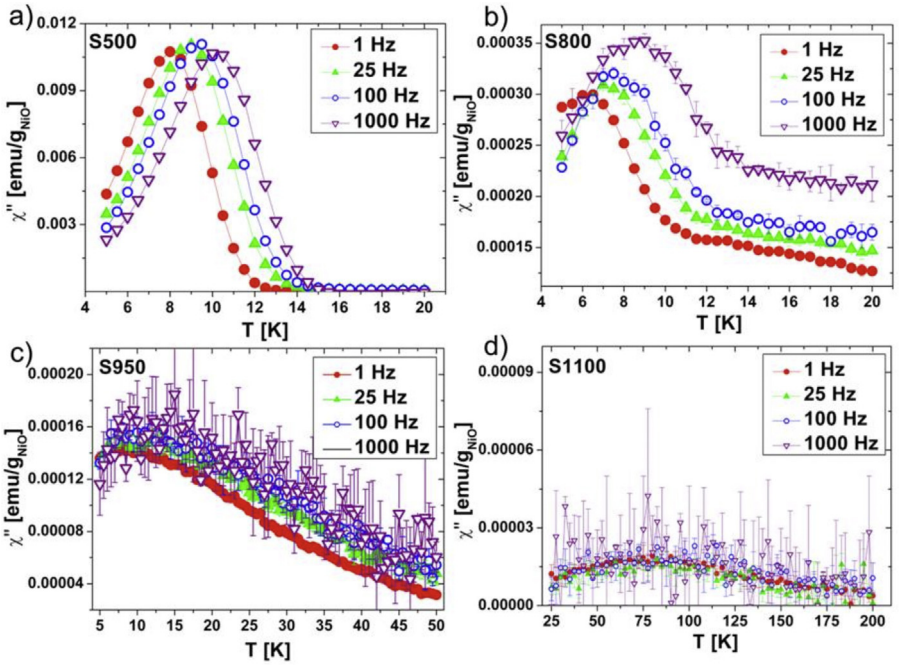

Fig. 10. Out-phase component of the AC susceptibility χ'' as a function of temperature for various frequencies for the samples S500 (a), S800 (b), S950 (c) and S1100 (d).

are the volumes of the nanoparticles in each sample. Using the values M_S = 7.63 emu/g and M_S = 4.21 emu/g measured at 100 K for the S500 and S800 nanoparticles, we obtained $m_{p(S500)} = 790\ \mu_B$ and $m_{p(S800)} = 593\ \mu_B$.

Magnetization as a function of applied magnetic field at four different temperatures is shown in Fig. 9 for S950 and S1100 samples. It can be seen that the behavior changes from superparamagnetic-like to a combination of ferromagnetic and antiferromagnetic-like. The observed coercivity is due to the uncompensated spins whereas the non-saturated behavior arises from antiferromagnetically ordered spins. It should be noted that the coercivity of the S1100 sample is much higher at low temperature ($H_{C(S1100)}$ = 5850 Oe at 5 K) compared to the other samples. At low temperature thermal energy is negligible and the measured coercivity indicates the energy barrier height, which is in agreement with the higher energy anisotropy E_a determined for S1100. It has been reported that the coercivity can be influenced by exchange or/and dipolar interactions due to an increase of the energy barrier [57]. We believe, based on the AC susceptibility and the suppressed FC magnetization increase, that inter-particle interactions play an important role in S1100. The observed decrease of magnetization M with increased annealing temperature of the NiO nanoparticles is due to the better crystallinity and increase in particle sizes as well as the demagnetizing character of inter-particle interactions [22]. Fig. 10 shows the out of phase AC susceptibility for all samples. It can be seen that the imaginary part of the susceptibility exhibits a peak in each case, in accordance with the DC magnetization and the real part of the AC susceptibility. The peak position shifts to higher temperatures with increasing frequency for S500 and S800 (Fig. 10(a–b)) as reported for nanosized systems. The measured imaginary susceptibilities for S950 and S1100 are noisy due to the smaller magnetic response of these samples. However, the existence of maxima can be observed below 20 K for S950 and below 100 K for S1100.

4. Conclusions

In summary, we have used XRPD, TEM and SQUID magnetometry to investigate the important influence of agglomeration on the magnetic properties of NiO nanoparticles embedded in a silica matrix and annealed at 500 °C (S500), 800 °C (S800), 950 °C (S950) and 1100 °C (S1100). TEM measurements revealed that both agglomerated and well-isolated nanoparticles coexist in the S800 sample, in contrast to the S500 sample where all the nanoparticles are well separated. The agglomeration likely occurs by the removal of thin parts of the silica matrix that separates nanoparticles in close proximity during annealing at 800 °C, enabling direct contact between nanoparticles. Both superparamagnetic and ferromagnetic-like behaviors are observed in the samples annealed at higher temperatures. The magnetic properties of S1100 show an abrupt increase of T_{max} and T_{irr}, indicating an increase in the size of the NiO particles. Moreover, we conclude that stronger inter-particle interactions increase the energy barrier and coercivity in the S1100 sample.

Acknowledgement

The Ministry of Education, Science and Technological Development of the Republic of Serbia supported this study financially (Grant no. III 45015).

References

[1] X. Luo, L.T. Tseng, S. Li, J.B. Yi, Room temperature ferromagnetic ordering of NiO films through exchange coupling, Mat. Sci. Semicon. Proc. 30 (2015) 228–232.
[2] S. Saravanakumar, R. Saravanan, S. Sasikumar, Effect of sintering temperature on the magnetic properties and charge density distribution of nano-NiO, Chem. Pap. 68 (6) (2014) 788–797.
[3] N. Rinaldi-Montes, P. Gorria, D. Martínez-Blanco, A.B. Fuertes, L. Fernández Barquín, J. Rodríguez Fernández, I. de Pedro, M.L. Fdez-Gubieda, J. Alonso, L. Olivi, G. Aquilanti, J.A. Blanco, Interplay between microstructure and magnetism in NiO nanoparticles: breakdown of the antiferromagnetic order, Nanoscale 6 (1) (2014) 457–465.
[4] M. Tadic, M. Panjan, D. Markovic, B. Stanojevic, D. Jovanovic, I. Milosevic, V. Spasojevic, NiO core–shell nanostructure with ferromagnetic-like behavior at room temperature, J. Alloys Comp. 586 (Suppl. 1) (2014) S322–S325.
[5] N. Bayal, P. Jeevanandam, Synthesis of SiO_2@ NiO magnetic core–shell nanoparticles and their use as adsorbents for the removal of methylene blue, J. Nanopart. Res. 15 (11) (2013) 1–15.
[6] W.J. Duan, S.H. Lu, Z.L. Wu, Y.S. Wang, Size effects on properties of NiO nanoparticles grown in alkalisalts, J. Phys. Chem. C 116 (49) (2012) 26043–26051.
[7] H. Gao, G. Daqiang, Z. Jing, Z. Zhaohui, Y. Guijin, S. Zhenhua, Z. Jinlin, Z. Zhonghua, X. Desheng, Synthesis and anomalous magnetic behaviour of NiO nanotubes and nanoparticles, Micro Nano Lett. 7 (1) (2012) 5–8.
[8] X.J. Yao, X.M. He, X.Y. Song, Q. Ding, Z.W. Li, W. Zhong, C.T. Au, Y.W. Du, Enhanced exchange bias and coercivity arising from heterojunctions in Ni–NiO nanocomposites, Phys. Chem. Chem. Phys. 16 (15) (2014) 6925–6930.
[9] K.O. Moura, R.J. Lima, A.A. Coelho, E.A. Souza-Junior, J.G. Duque, C.T. Meneses, Tuning the surface anisotropy in Fe-doped NiO nanoparticles, Nanoscale 6 (1) (2014) 352–357.
[10] Q. Dong, S. Yin, C. Guo, X. Wu, N. Kumada, T. Takei, A. Miura, Y. Yonesaki, T. Sato, Single-crystalline porous NiO nanosheets prepared from β-Ni $(OH)_2$ nanosheets: magnetic property and photocatalytic activity, Appl. Catal. B –Environ. 147 (2014) 741–747.
[11] M. Tadić, M. Panjan, D. Marković, I. Milošević, V. Spasojević, Unusual magnetic properties of NiO nanoparticles embedded in a silica matrix, J. Alloys Compd. 509 (25) (2011) 7134–7138.
[12] S.D. Pappas, A. Delimitis, V. Kapaklis, E.T. Papaioannou, P. Poulopoulos, D. Trachylis, M.J. Velgakis, C. Politis, Natural nanomorphous Ni/NiO magnetic multilayers: structure and magnetism of the high-Ar pressure series, J. Nanosci. Nanotechnol. 14 (8) (2014) 6103–6107.
[13] S.D. Tiwari, K.P. Rajeev, Effect of distributed particle magnetic moments on the magnetization of NiO nanoparticles, Solid State Commun. 152 (12) (2012) 1080–1083.
[14] M. Tadić, M. Panjan, D. Marković, NiO/SiO_2 nanostructure and the magnetic moment of NiO nanoparticles, Mater. Lett. 64 (19) (2010) 2129–2131.
[15] S. D'Addato, M.C. Spadaro, P. Luches, V. Grillo, S. Frabboni, S. Valeri, A.M. Ferretti, E. Capetti, A. Ponti, Controlled growth of Ni/NiO core–shell nanoparticles: structure, morphology and tuning of magnetic properties, Appl. Surf. Sci. 306 (2014) 2–6.
[16] B. Kisan, P.C. Shyni, S. Layek, H.C. Verma, D. Hesp, V. Dhanak, S. Krishnamurthy, A. Perumal, Finite size effects in magnetic and optical properties of antiferromagnetic NiO nanoparticles, IEEE Trans. Magn. 50 (1) (2014) 1–4.
[17] I. Sugiyama, N. Shibata, Z. Wang, S. Kobayashi, T. Yamamoto, Y. Ikuhara, Ferromagnetic dislocations in antiferromagnetic NiO, Nat. Nanotechnol. 8 (4) (2013) 266–270.
[18] F.H. Aragón, P.E.N. de Souza, J.A.H. Coaquira, P. Hidalgo, D. Gouvêa, Spin-glass-like behavior of uncompensated surface spins in NiO nanoparticulated powder, Physica B 407 (13) (2012) 2601–2605.
[19] J.F.K. Cooper, A. Ionescu, R.M. Langford, K.R.A. Ziebeck, C.H.W. Barnes, R. Gruar, C. Tighe, J.A. Darr, N.T.K. Thanh, B. Ouladdiaf, Core/shell magnetism in NiO nanoparticles, J. Appl. Phys. 114 (8) (2013) 083906.
[20] V. Bisht, K.P. Rajeev, Memory and aging effects in NiO nanoparticles, J. Phys.-Condens. Mat. 22 (1) (2010) 016003.
[21] H.N. Duan, S.L. Yuan, X.F. Zheng, Z.M. Tian, The synthesis and exchange bias effect of monodisperse NiO nanocrystals, Chin. Phys. B 21 (7) (2012) 078101.
[22] E. Winkler, R.D. Zysler, M. Vasquez Mansilla, D. Fiorani, D. Rinaldi, M. Vasilakaki, K.N. Trohidou, Surface spin-glass freezing in interacting core–shell NiO nanoparticles, Nanotechnology 19 (18) (2008) 185702.
[23] J.B. Yi, J. Ding, Y.P. Feng, G.W. Peng, G.M. Chow, Y. Kawazoe, B.H. Liu, J.H. Yin, S. Thongmee, Size-dependent magnetism and spin-glass behavior of amorphous NiO bulk, clusters, and nanocrystals: experiments and first-principles calculations, Phys. Rev. B 76 (22) (2007), 224402.
[24] Z. Yang, D. Gao, K. Tao, J. Zhang, Z. Shi, Q. Xu, S. Shi, D. Xue, A series of unexpected ferromagnetic behaviors based on the surface-vacancy state: an insight into NiO nanoparticles with a core–shell structure, RSC Adv. 4 (86) (2014) 46133–46140.
[25] S.D. Tiwari, K.P. Rajeev, Signatures of spin-glass freezing in NiO nanoparticles, Phys. Rev. B 72 (10) (2005) 104433.
[26] Y. Cui, C. Wang, S. Wu, G. Liu, F. Zhang, T. Wang, Lotus-root-like NiO nanosheets and flower-like NiO microspheres: synthesis and magnetic properties, CrystEngComm 13 (15) (2011) 4930–4934.
[27] E. Winkler, R.D. Zysler, M. Vasquez Mansilla, D. Fiorani, Surface anisotropy effects in NiO nanoparticles, Phys. Rev. B 72 (13) (2005), 132409.
[28] M.P. Proenca, C.T. Sousa, A.M. Pereira, P.B. Tavares, J. Ventura, M. Vazquez, J.P. Araujo, Size and surface effects on the magnetic properties of NiO nanoparticles, Phys. Chem. Chem. Phys. 13 (20) (2011) 9561–9567.

[29] M.N. Carneiro, W.C. Nunes, R.P. Borges, M. Godinho, L.E. Fernandez-Outon, W.A.A. Macedo, I.O. Mazali, NiO nanoparticles dispersed in mesoporous silica glass, J. Phys. Chem. C 114 (44) (2010) 18773–18778.
[30] H. Shim, A. Manivannan, M.S. Seehra, K.M. Reddy, A. Punnoose, Effect of interparticle interaction on the magnetic relaxation in NiO nanorods, J. Appl. Phys. 99 (8) (2006) 08Q503.
[31] F. Bødker, M.F. Hansen, C. Bender Koch, S. Mørup, Particle interaction effects in antiferromagnetic NiO nanoparticles, J. Magn. Magn. Mater. 221 (1–2) (2000) 32–36.
[32] C.T. Meneses, J.G.S. Duque, E. de Biasi, W.C. Nunes, S.K. Sharma, M. Knobel, Competing interparticle interactions and surface anisotropy in NiO nanoparticles, J. Appl. Phys. 108 (1) (2010) 013909.
[33] V. Zelenak, A. Zelenakova, J. Kovac, U. Vainio, N. Murafa, Influence of surface effects on magnetic behavior of hematite nanoparticles embedded in porous silica matrix, J. Phys. Chem. C 113 (30) (2009) 13045–13050.
[34] M. Tadic, V. Kusigerski, D. Markovic, I. Milosevic, V. Spasojevic, High concentration of hematite nanoparticles in a silica matrix: structural and magnetic properties, J. Magn. Magn. Mater. 321 (1) (2009) 12–16.
[35] Y. El Mendili, J.-F. Bardeau, F. Grasset, J.-M. Greneche, O. Cador, T. Guizouarn, N. Randrianantoandro, Magnetic interactions in γ-Fe_2O_3@SiO_2 nanocomposites, J. Appl. Phys. 116 (5) (2014) 053905.
[36] K. Nadeem, F. Zeb, M. Azeem Abid, M. Mumtaz, M. Anis ur Rehman, Effect of amorphous silica matrix on structural, magnetic, and dielectric properties of cobalt ferrite/silica nanocomposites, J. Non-Cryst. Solids 400 (2014) 45–50.
[37] S.H. Xiao, K. Luo, L. Zhang, The structural and magnetic properties of cobalt ferrite nanoparticles formed in situ in silica matrix, Mater. Chem. Phys. 123 (2–3) (2010) 385–389.
[38] A. Parma, I. Freris, P. Riello, D. Cristofori, C. de Julián Fernández, V. Amendola, M. Meneghetti, A. Benedetti, Structural and magnetic properties of mesoporous SiO_2 nanoparticles impregnated with iron oxide or cobalt-iron oxide nanocrystals, J. Mater. Chem. 22 (36) (2012) 19276–19288.
[39] T.P. Braga, A.N. Pinheiro, W.T. Herrera, Y.T. Xing, E. Baggio-Saitovitch, A. Valentini, Synthesis and characterization of iron oxide nanoparticles dispersed in mesoporous aluminum oxide or silicon oxide, J. Mater. Sci. 46 (3) (2011) 766–773.
[40] I. Ursachi, A. Vasil, A. Ianculescu, E. Vasile, A. Stancu, Ultrasonic-assisted synthesis and magnetic studies of iron oxide/MCM-41 nanocomposite, Mater. Chem. Phys. 130 (3) (2011) 1251–1259.
[41] Y. Wang, J. He, J. Chen, L. Ren, B. Jiang, J. Zhao, Synthesis of monodisperse, hierarchically mesoporous, silica microspheres embedded with magnetic nanoparticles, ACS Appl. Mater. Interfaces 4 (5) (2012) 2735–2742.
[42] L. Xu, H. Huang, S. Tang, L. Chen, R. Xie, W. Xia, J. Wei, W. Zhong, Y. Du, Facile synthesis of nickel nanoparticles supported on carbon and silica matrix via a novel silica sol–gel process, J. Sol–Gel Sci. Technol. 69 (1) (2014) 130–136.
[43] A.C. Gandhi, J. Pant, S.D. Pandit, S.K. Dalimbkar, T.S. Chan, C.L. Cheng, Y.R. Ma, S.Y. Wu, Short-range magnon excitation in NiO nanoparticles, J. Phys. Chem. C 117 (36) (2013) 18666–18674.
[44] T. Tajiri, S. Saisho, M. Mito, H. Deguchi, K. Konishi, A. Kohno, Size dependence of crystal structure and magnetic properties of NiO nanoparticles in mesoporous silica, J. Phys. Chem. C 119 (2) (2015) 1194–1200.
[45] Larson A.C. and von Dreele R.B. General Structure Analysis System (GSAS), Los Alamos National Laboratory LAUR Report 2004, No. 86-748.
[46] G. Compagnini, L. D'Urso, C. Spinella, O. Puglisi, Formation and characterization of high-density silver nanoparticles embedded in silica thin films by "in situ" self-reduction, J. Mater. Res. 16 (2001) 2934–2938.
[47] J.A. Mydosh, Spin Glasses, Taylor and Francis, Washington, 1993.
[48] M. Tadic, V. Kusigerski, D. Markovic, M. Panjan, I. Milosevic, V. Spasojevic, Highly crystalline superparamagnetic iron oxide nanoparticles (SPION) in a silica matrix, J. Alloys Compd. 525 (2012) 28–33.
[49] H. Shim, P. Dutta, M.S. Seehra, J. Bonevich, Size dependence of the blocking temperatures and electron magnetic resonance spectra in NiO nanoparticles, Solid State Commun. 145 (4) (2008) 192–196.
[50] M. Tadic, S. Kralj, M. Jagodic, D. Hanzel, D. Makovec, Magnetic properties of novel superparamagnetic iron oxide nanoclusters and their peculiarity under annealing treatment, Appl. Surf. Sci. 322 (2014) 255–264.
[51] C. Vázquez-Vázquez, M.A. López-Quintela, M.C. Bujan-Nunez, J. Rivas, Finite size and surface effects on the magnetic properties of cobalt ferrite nanoparticles, J. Nanopart. Res. 13 (4) (1663-1676).
[52] A. Zeleňáková, J. Kováč, V. Zeleňák, Magnetic properties of Fe_2O_3 nanoparticles embedded in hollows of periodic nanoporous silica, J. Appl. Phys. 108 (3) (2010) 034323.
[53] K. Rumpf, P. Granitzer, P. Poelt, M. Reissner, Specific loading of porous silicon with iron oxide nanoparticles to achieve different blocking temperatures, Thin Solid Films 543 (2013) 56–58.
[54] P.H. Linh, D.H. Manh, P.T. Phong, L.V. Hong, N.X. Phuc, Magnetic properties of Fe_3O_4 nanoparticles synthesized by coprecipitation method, J. Supercond Nov. Magn. 27 (9) (2014) 2111–2115.
[55] J. Landers, F. Stromberg, M. Darbandi, C. Schöppner, W. Keune, H. Wende, Correlation of superparamagnetic relaxation with magnetic dipole interaction in capped iron-oxide nanoparticles, J Phys: Condens. Matter. 27 (2) (2015) 026002.
[56] S. Bullita, A. Casu, M.F. Casula, G. Concas, F. Congiu, A. Corrias, A. Falqui, D. Loche, C. Marras, $ZnFe_2O_4$ nanoparticles dispersed in a highly porous silica aerogel matrix: a magnetic study, Phys. Chem. Chem. Phys. 16 (10) (2014) 4843–4852.
[57] M. Tadić, V. Kusigerski, D. Marković, M. Panjan, I. Milošević, V. Spasojević, Highly crystalline superparamagnetic iron oxide nanoparticles (SPION) in a silica matrix, J. Alloy Compd. 525 (2012) 28–33.
[58] K. Nadeem, H. Krenn, T. Traussnig, R. Würschum, D.V. Szabó, I. Letofsky-Papst, Effect of dipolar and exchange interactions on magnetic blocking of maghemite nanoparticles, J. Magn. Magn. Mater. 323 (15) (2011) 1998–2004.